Analysis of Excavation Shapes on Fully Grouted Rock Bolt using EFEM

Debasis Deb
Kamal C. Das
Sandeep Kavala

Department of Mining Engineering
IIT Kharagpur-721302, India
Email: deb@iitkgp.ac.in

ABSTRACT

Rock bolts have been widely used as a primary support system to stabilize rock masses around tunnel, underground mine galleries, slopes and others structures. A new numerical procedure called enriched finite element method (EFEM) has been developed by the authors for analysis of the interaction mechanism of rock and fully grouted bolt. This paper quantitatively evaluates bolt performance in different shape of underground opening *viz* circular, rectangular and D-shaped, using the proposed enriched finite element method (EFEM) combined with elasto-plastic behaviour of rock mass and grout material. In addition, comparative study of bolt performance is also presented considering both coupled and decoupled behaviour of rock bolts.

Keywords: Rock bolt performance; Underground opening shape; EFEM; DEFEM.

1. INTRODUCTION

Rock bolts have been widely used as a primary support system to stabilize slopes, hydro dams and underground structures such as tunnels and mine workings and other structures made in rock masses. The term "rock bolt" is defined in geomechanics as a form of mechanical support that is inserted into the rock mass with the primary objective of increasing its stiffness and/or strength with respect to tensile or shear loads. In general, rock bolts reinforce rock masses through restraining the deformation within rock masses (Li and Stillborg, 1999) and reduces the yield region around the excavation boundary. During the last four decades, different types of rock bolts have been practiced, out of which fully grouted active/passive bolts were the most common types. For a fully grouted passive rock bolt installed in deformable rock masses, a neutral point exist on the bolt rod, where shear stress at the interface between the bolt and grout material vanishes. Based on neutral point concepts, shear stresses and axial loads developed along a bolt rod are analytically formulated by many researchers (Li and Stillborg, 1999; Hyett et al., 1996). Bolt grout interactions around a circular tunnel in Hoek-Brown medium have been formulated analytically considering a bolt density factor (Indraratna and Kaiser, 1991). Considering different approaches to bolt performance Stille et al., (1989) presented a closed form elasto-plastic analytical

solutions of grouted bolts. Based on shear lag model (SLM), Cai et al. (2004) derived an analytical solution of rock bolts for describing the interaction behaviours of rock bolt, grout material and rock mass. Brady and Lorig (1988) numerically analyzed the interactions of bolt grout in Mohr Columb media using finite difference method (FDM) technique.

In addition, numerous studies have been published on the analytical solution of stresses and displacements around a circular tunnel considering elasto-plastic rock mass with Mohr-Coulomb yield criterion (Carranza-Torres and Fairhurst, 1999; Carranza-Torres,2004; Sharan, 2003; Deb and Choi, 2005). Elwi and Hrudey (1989) and d'Avila et al.,(2008) proposed embedded finite element method for reinforcing curved layers and concrete structures respectively. Finite Element Method (FEM) and/or FDM based procedures are also developed for the analysis of the said problem and have been presented in many references for solving geotechnical problems (Deb, 2006; Pande et al., 1990; Rocscience, 2005; Itasca, 2005; Goodman et al., 1968; Crotty and Wardle, 1985; Cundall, 1971). In FEM framework, limited works have been published for analysis of the interaction between fully grouted rock bolt and elasto-plastic rock mass. Few literatures have dealt with finite element procedure involving combination of decoupled rock bolts and elasto-plastic rock mass. In some cases, bolt needs to be aligned along finite element nodes causing difficulty in mesh generation (Rocscience, 2005).

Recently, a new method called "enriched finite element method (EFEM)" has been proposed by authors (Deb and Das, 2010) based on the interaction mechanism between rock bolt and rock mass to assess effect of bolting on rock mass behaviour and bolt performance for a circular tunnel. Concept of "enriched element" has been introduced in which a bolt can intersect a regular element at any arbitrary direction. Each node of an "enriched element" has additional degrees of freedom to determine displacements and stresses of the bolt rod. The stiffness of an enriched element comprises constitutive properties of rock mass, physical and material properties of bolt and grout, orientation of bolt and borehole diameter. The enriched element can be applied for analysis of elasto-plastic rock mass. The influence of the coupling and decoupling behaviour between the reinforcement and surrounding rock mass has also been taken into account.

This paper quantitatively evaluates bolt performance for different shape of underground opening viz circular, rectangular and D-shaped using proposed enriched finite element method (EFEM). The EFEM procedure has been applied to compute shear stress and axial load along the bolt length for each bolt installed at different locations of these excavation geometries. In this paper, both coupled and decoupled behaviour of rock bolts have been studied and results are compared for different excavation geometries.

2. MECHANISMS OF GROUTED ROCK BOLT SYSTEM

The performance of any reinforcement system is limited by the efficiency of load transfer, a process that begins when a block of reinforced rock moves. The concepts of load transformation from weaker or unstable to stronger or stable rock mass to prevent

possible failure or collapse comprises three basic mechanisms (Stille, 1992; Windsor and Thompson, 1993):

(a) Rock movement, which requires load transfer from unstable rock to the bolt.
(b) Transfer of load via bolts from an unstable zone to a stable zone.
(c) Transfer of the bolt load to a stable rock mass.

There are wide varieties of methods by which the load transfer between rock and bolt element may be achieved. Windsor and Thomson (1993, 1996) refined these concepts as the transformation of load from unstable rock within the reinforcement system to stable rock. They classified the current reinforcement system into three groups:

(a) Continuous mechanically coupled (CMC),
(b) Continuous frictionally coupled (CFC) and
(c) Discretely mechanical or frictionally coupled (DMFC).

A fully grouted rock bolt is a passive support system, which is activated by movement of the surrounding rock mass. Fully grouted bolting consists of bolt, grout, and surrounding rock mass. The relationship between them is similar to the continuous mechanically coupled (CMC) bolt system, shown in Fig. 1. The efficiency of load transfer is affected by the type and properties of the grout, profile of the rock bolt, hole and bolt diameter, anchorage length, rock material, confinement pressure, and installation procedures. As Fig. 1 shows, a fully grouted bolt provides greater shear surface for transmitting the load from rock to bolt and vice versa (Snyder, 1983). The grout supplies a mechanism for transferring load between the rock and reinforcing element. This redistribution of stresses along the bolt is the result of movement in the rock mass, which transfer the load to the bolt via shear resistance in the grout.

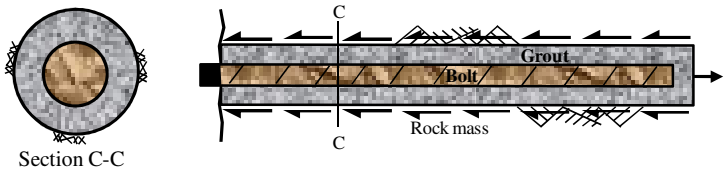

Fig. 1 - Load transfer in continuous mechanically coupled (fully grouted) rock bolt

Interaction mechanism of rock bolt and rock mass is described according to their consistent displacement. The EFEM models (Deb and Das, 2010) are developed to predict the distribution of axial force and shear stress along the rock bolt considering bolt coupling and decoupling behaviours. According to the analysis, force developed along the bolt length is related to the displacement of surrounding rock mass. The assumptions of EFEM procedure is given in references (Deb and Das, 2010; Marence and Swoboda, 1995).

3. ENRICHED FINITE ELEMENT PROCEDURE

The enriched finite element procedure has been developed and introduced for grouted bolt in the similar way as extended finite element method applied to jointed rock mass

((Deb and Das, 2009; Deb and Das, 2010b). In X-FEM, displacement discontinuity along joint plane is represented by 'Heaviside' enrichment functions. In EFEM, displacement discontinuity (non-zero relative displacement at rock-grout interface) along rock-grout interface takes place and hence load developed in the bolt. The governing equation for grouted rock bolt in terms of displacement along bolt length is described by the second order inhomogeneous linear ordinary differential equation as:

$$\frac{d^2u_b}{dx^2}+\frac{k}{A_bE_b}\left(u_r-u_b\right)=0 \tag{1}$$

where A_b = bolt cross sectional area, E_b = bolt modulus of elasticity, k = shear stiffness of grout material and generally depends on grout properties, geometry of the bolt, borehole and spacing of bolts (Marence and Swoboda, 1995) and u_r and u_b are displacements corresponding to rock and bolt rod respectively. Equation (1) suggests that the solution of u_b can be obtained if u_r is known beforehand. In this study, the solutions are obtained from the nodal displacements of the proposed EFEM model with bolts installed at the excavation boundary.

3.1 Discretized Enriched Finite Element Equations

As mentioned earlier, an element intersected by a bolt is termed as 'enriched element'. Let's assume that a bolt is intersected a 3-noded triangular element at an angle α with the x axis as shown in Fig. 2. The nodal displacements vectors of rock mass and bolt are denoted by $[u_{ri} \quad v_{ri}]^T$ and $[u_{bi} \quad v_{bi}]^T$ respectively. The characteristics of this element differ from those of regular 3-noded element, since 2 additional degrees of freedom are incorporated at every node to obtain displacements of bolt rod in *x* and *y* directions. In a finite element mesh, elements which are not intersected by a bolt are treated as 'regular elements'.

Stiffness matrix of enriched element is formulated in $x'-y'$ coordinate system and it is transformed into global $x-y$ coordinates system before it can be added with stiffness matrix of rock mass.

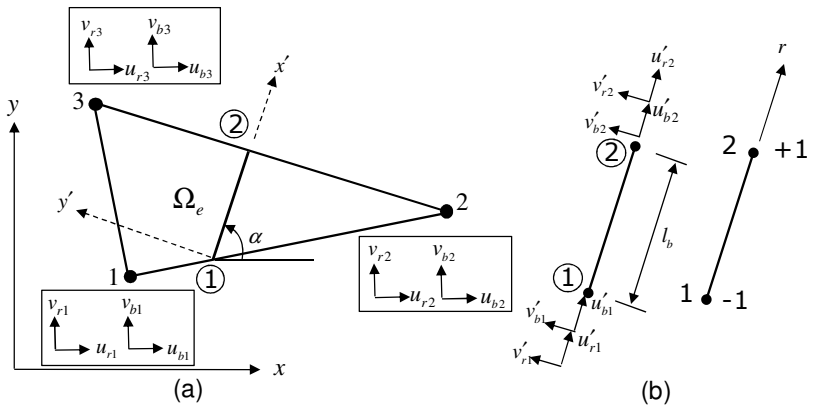

Fig. 2 - Enriched constant strain triangle (a) 3-noded triangular element intersected by a bolt (b) bolt element in local coordinate system

3.2 Stiffness Matrix in Local (Bolt) Coordinate System

In EFEM procedure, the combined stiffness matrix in $x'-y'$ coordinate system has been derived based on 8 degrees of freedom comprising displacements of rock as $[u'_{r1} \quad v'_{r1} \quad u'_{r2} \quad v'_{r2}]^T$ and those of bolt as $[u'_{b1} \quad v'_{b1} \quad u'_{b2} \quad v'_{b2}]^T$, where subscript 1 and 2 denote the intersection points as mentioned in Fig. 2. The stiffness matrix is written in the form of

$$\mathbf{K}' = \begin{bmatrix} \mathbf{K}'_{rr} & \mathbf{K}'_{rb} \\ \mathbf{K}'_{br} & \mathbf{K}'_{bb} \end{bmatrix} \tag{2}$$

where $\mathbf{K}'$ is a symmetric 8×8 square matrix and each components matrices are 4×4 square matrix. The component matrices are given below (Deb and Das, 2010):

$$\mathbf{K}'_{rr} = A_b \int_{\Gamma_b} \mathbf{H}_r^T G_b \mathbf{H}_r \mathrm{d}\Gamma + \int_{\Gamma_b} \mathbf{P}_r^T k \mathbf{P}_r \mathrm{d}\Gamma \tag{3a}$$

$$\mathbf{K}'_{rb} = -\int_{\Gamma_b} \mathbf{P}_r^T k \mathbf{P}_b \mathrm{d}\Gamma \tag{3b}$$

$$\mathbf{K}'_{br} = -\int_{\Gamma_b} \mathbf{P}_b^T k \mathbf{P}_r \mathrm{d}\Gamma \tag{3c}$$

$$\mathbf{K}'_{bb} = A_b \int_{\Gamma_b} \mathbf{H}_b^T E_b \mathbf{H}_b \mathrm{d}\Gamma + \int_{\Gamma_b} \mathbf{P}_b^T k \mathbf{P}_b \mathrm{d}\Gamma \tag{3d}$$

where $\mathbf{H}_r$ and $\mathbf{H}_b$ are one dimensional (along axial direction) strain-displacement matrices, $\mathbf{P}_r^T = \mathbf{P}_b^T$ denote the interpolation matrix of intersection points (1) and (2) of the bolt element as shown in Fig. 2(b).

3.3 Transformation of Stiffness Matrix in Global Coordinate System

The stiffness matrix given in Eq. (2) is transformed into global $x-y$ coordinates system before it is added with the stiffness matrix of rock mass. Hence, the combined stiffness matrix of dimension $4n\times4n$ of an enriched element becomes

$$\mathbf{K}_{en} = \begin{bmatrix} \mathbf{K}_{rr} & \mathbf{K}_{rb} \\ \mathbf{K}_{br} & \mathbf{K}_{bb} \end{bmatrix} \tag{4}$$

where each components matrices of $\mathbf{K}_{en}$ of dimension $2n\times2n$ are

$$\mathbf{K}_{rr} = \int_{\Omega} \mathbf{B}_r^T \mathbf{D} \mathbf{B}_r \mathrm{d}\Omega + \mathbf{M}_1^T \mathbf{T}_c^T \mathbf{K}'_{rr} \mathbf{T}_c \mathbf{M}_1 \tag{5a}$$

$$\mathbf{K}_{rb} = \mathbf{M}_1^T \mathbf{T}_c^T \mathbf{K}'_{rb} \mathbf{T}_c \mathbf{M}_1 \tag{5b}$$

$$\mathbf{K}_{br} = \mathbf{M}_1^T \mathbf{T}_c^T \mathbf{K}'_{br} \mathbf{T}_c \mathbf{M}_1 \tag{5c}$$

$$\mathbf{K}_{bb} = \mathbf{M}_1^T \mathbf{T}_c^T \mathbf{K}'_{bb} \mathbf{T}_c \mathbf{M}_1 \tag{5d}$$

where $\mathbf{T} = \begin{bmatrix} \mathbf{T}_c & \mathbf{0} \\ \mathbf{0} & \mathbf{T}_c \end{bmatrix}$ transformation matrix and $\mathbf{M} = \begin{bmatrix} \mathbf{M}_1 & \mathbf{0} \\ \mathbf{0} & \mathbf{M}_1 \end{bmatrix}_{8\times4n}$ denotes the matrix of shape.

3.4 Mohr-Coulomb Yield Criterion for Rock Mass

Mohr-Coulomb yield criterion is popularly applied in rock mechanics to determine the onset of yielding. In EFEM procedure, rock mass failure is considered based on the

concept that yielding occurs when a critical combination of the shear stress and mean normal stress is reached (Deb and Das, 2010).

3.5 Decoupling between Bolt Rod and Grout Material

Grout material may yield/fail if shear stress at grout-bolt interface exceeds the peak shear strength of the material. In this case, the yield function is assumed as

$$F = |\tau| - \tau_p = 0 \tag{6}$$

where $\tau = ku_s / 2\pi r_b$ and τ_p denotes the peak shear strength of grout material. If F is positive, decoupling occurs at the bolt-grout interface. Shear stress increases with shear displacement (u_s) until peak strength (τ_p) is reached. Henceforth, shear stress decreases with further increase in shear displacement and ultimately reaches to residual value (τ_r) as shown schematically in Fig. 3(a). In case of shear yielding (decoupling), the displacement increment (Δu_s) is divided into elastic and plastic parts as

$$\Delta u_s = \Delta u_s^e + \Delta u_s^p \tag{7}$$

In this study, elastic-perfectly plastic condition is assumed and hence, $\Delta u_s^e = 0$ after yielding of grout. The plastic displacement increment is then added into the effective cumulative plastic-displacement (u_s^{eff}) as

$$u_s^{eff} = u_s^{eff} + |\Delta u_s^p| \tag{8}$$

In iterative Newton-Raphson solution scheme, shear strength (τ_p) and shear modulus (G_g) of grout material for next iteration are reduced based on u_s^{eff} of the current load step as shown schematically in Fig. 3(b). The updated G_g and are then applied for the next iteration cycle.

3.6 Implementation Procedure of EFEM

The above numerical procedures are implemented using 3-noded triangular element and can easily be extended for higher order elements. From the definition of enriched element, it is clear that all nodes of that element are also enriched. Each enriched node has 4 degrees of freedom; 2 for rock mass and other 2 for bolt rod.

Initially, the stiffness matrix given in Eq. (4) is evaluated considering the elastic properties of the rock material, bolt-grout properties and orientation of the bolt. The essential boundary conditions are applied depending on the problem statement. Then, load is incremented and solution of nodal displacements are sought. Strains and stresses at Gauss points are also updated based on the incremental displacements. The unbalanced forces those may develop due to yielding of rock mass and/ or decoupling of bolt are determined using Eq. (6) and full Newton-Raphson solution scheme is applied to obtain the converged solution. Once the solution is converged, load is again incremented and the same procedure is continued.

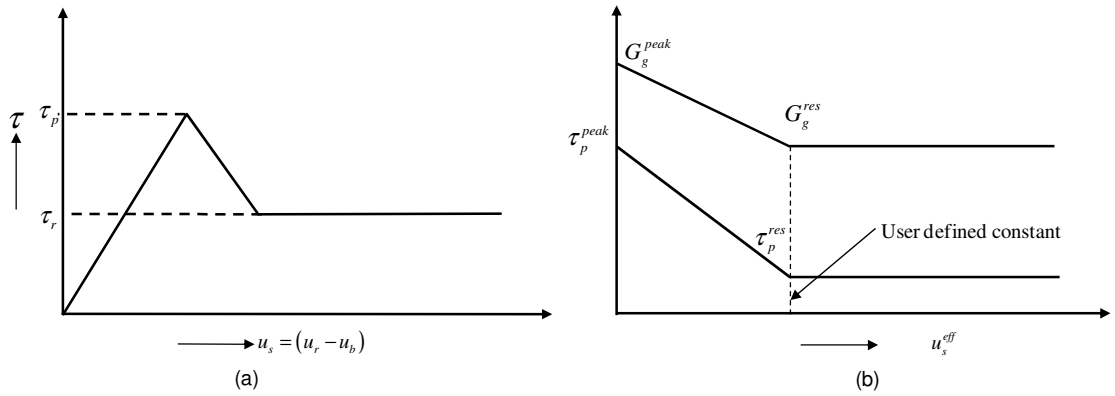

Fig. 3 - (a) Shear stress falls and attains a residual, (b) Shear modulus falls of grout material

4. NUMERICAL EXAMPLES

Among various shapes of underground openings, circular and D-shape (or horseshoe) tunnels are the most popular in hydro-electric, railway and road projects, while rectangular tunnels are common in mining sectors. In this study, these 3 shapes of underground opening have been considered for the analysis as shown in Figs. 5(a)–(c). All models are analyzed in plane strain condition having hydrostatic far field stress (p_0) of 8.0MPa. Numerical examples have been performed considering first coupled bolt with elastic rock mass and then decoupled bolt with elasto-plastic rock mass. The geomechanical and Mohr-Coulomb parameters of the rock masses are listed in Table 1. Rock bolt parameters are listed in Table 2. In earlier work by the authors (Deb and Das, 2010) has shown that a bolt length of 4 m is suitable for supporting a circular tunnel of 4.75m radius with similar geological conditions. In this study, all numerical models are analyzed considering equivalent area of the opening (shown in Fig. 5) with 4m of bolt length. The initial stiffness scheme is adopted for solving displacements using Newton-Raphson method.

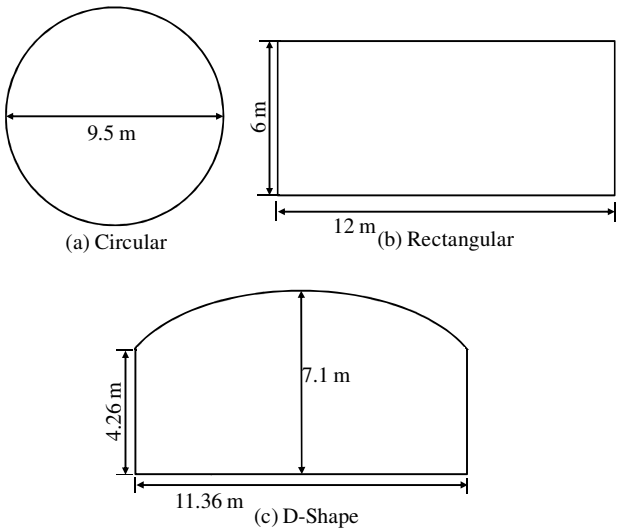

Fig. 5 - Three different shapes of underground openings considered for the analysis

Table 1 - Rock mass properties

E (GPa)	ν	C (MPa)	φ (deg)	ψ (deg)	c_r (MPa)	φ_r (deg)	ψ_r (deg)	Tensile strength (MPa)
5.0	0.25	1.5	30.0	20.0	0.5	20.0	10.0	1.0

C: cohesion, φ : angle of internal friction

Table 2 - Parameters of rock bolt

r_b (mm)	r_h (mm)	E_b (GPa)	G_b (GPa)	G_g (GPa)	τ_p (MPa)	τ_r(Mpa)	G_g^r(GPa)
10.0	20.0	210.0	84.0	1.0	5.0	1.0	0.1

4.1 Circular Tunnel

A bolted circular tunnel of 4.75 m radius with 8 bolts installed at regular circumferential spacing of 1.24 m or every 11.125^0 interval from the horizontal. The geometry of the model, finite element mesh and boundary conditions are shown in Fig. 6. Finer mesh is developed near the tunnel boundary for improving the accuracy of results. Since the problem is axisymmetric, it is sufficient to analyze only one quarter of the tunnel. The models are made up with 2358 CST elements having 1254 nodes.

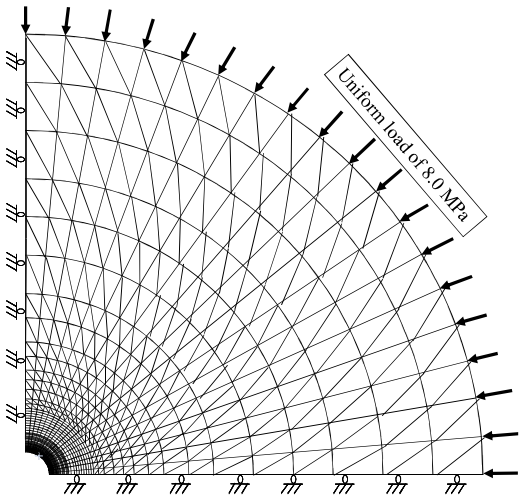

Fig. 6 - Meshed circular tunnel with uniform far field stress and boundary conditions

4.1.1 Results and discussions

Figures 7(a) and 8(a) depicts the bolt axial force and shear stress obtained along the bolt length for elastic rock mass and coupled bolt. The sense of the shear stress on the bolt section close to the tunnel wall is negative, which means that the bolt is pulled towards the tunnel boundary. The neutral point is located at 0.42 m from the tunnel

wall (Fig. 7(a)). The axial force in the bolt rod is the maximum at the neutral point and decreases to zero towards each ends of the bolt. The maximum axial force of 101.2 kN is obtained for coupled bolts with elastic rock mass. The distribution of shear stress and axial force along the decoupled bolt with elasto-plastic rock mass are illustrated in Figs. 7(b) and 8(b). The shear failure at the bolt-grout interface would result in a release of the restrained rock deformation at near end of the tunnel boundary. After decoupling, location of neutral point moves to 1.2 m inside the rock mass from the tunnel wall. The shear stress attains residual value at decoupled zone as shown in Fig. 8(b). The maximum axial force increases to 186 kN at the neutral point due to more deformation in the rock mass. This indicates that, rock mass fails near the excavation boundary causing higher displacements/axial force in the bolt. It can also be seen from Figs. 7 and 8, bolt axial force and shear stress behaviour are independent on its position for a circular tunnel due to symmetric distribution of stresses and displacement around the tunnel opening. The shear stress and axial force obtained from this study reflect the similar pattern those mentioned in the references of Li and Stillborg (1999) and Cai et al. (2004).

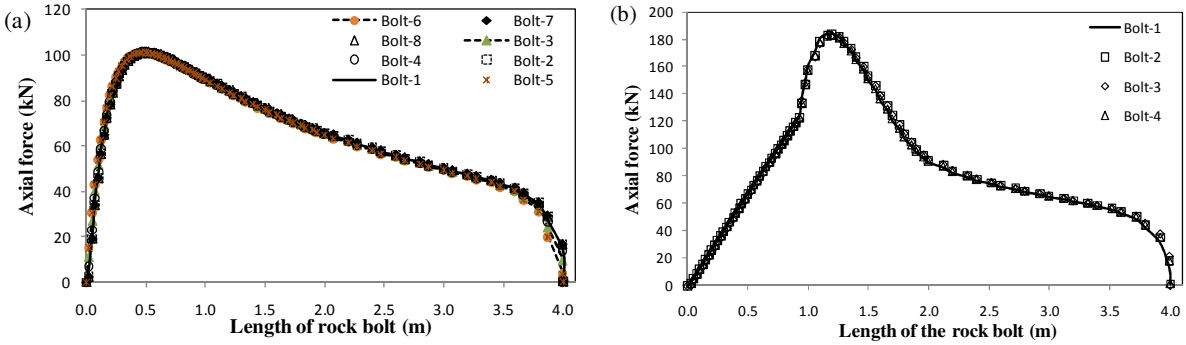

Fig. 7 - Distribution of axial force on (a) coupled rock bolt and elastic rock mass (b) decoupled rock bolt and elasto-plastic rock mass around a circular opening

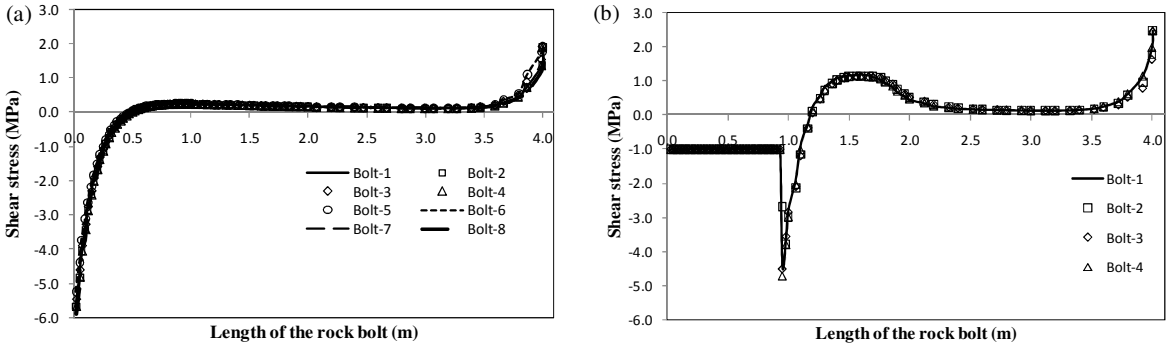

Fig. 8 - Distribution of shear stress on (a) coupled rock bolt and elastic rock mass (b) decoupled rock bolt and elasto-plastic rock mass around a circular opening

4.2 Rectangular Tunnel

In this example, a rectangular tunnel of 12 m width and 6 m height has been considered keeping almost the same excavation area as circular tunnel. The geometry of the model, finite element mesh and boundary conditions are shown in Fig. 9. Finer mesh is

developed near the tunnel boundary for improving the accuracy of results. Since the problem is axisymmetric, it is sufficient to analyze only one quarter of the rectangular tunnel. The models are developed with 4699 CST elements having 2429 nodes and 8 bolts installed at regular interval from the horizontal axis. Bolts positions are shown in Fig. 10(a) (inset-left top).

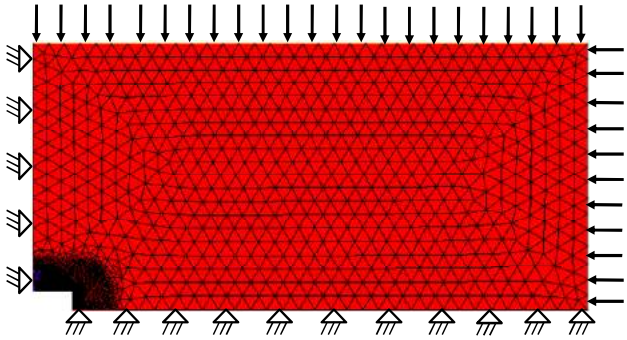

Fig. 9 - FE meshed for rectangular tunnel with uniform far field stress and boundary conditions

4.2.1 Results and discussions

Figures 10(a) and 11(a) depicts the bolt axial force and shear stress obtained along the bolt length for elastic rock mass and coupled bolts. As before, the sense of the shear stress on the bolt section close to the tunnel wall is negative which means that the bolt is pulled towards the tunnel boundary. In this case, location of neutral point and the maximum axial force depends on the bolt location and orientation. The position of neutral point and maximum axial force for corresponding bolt number are given in Table 3.

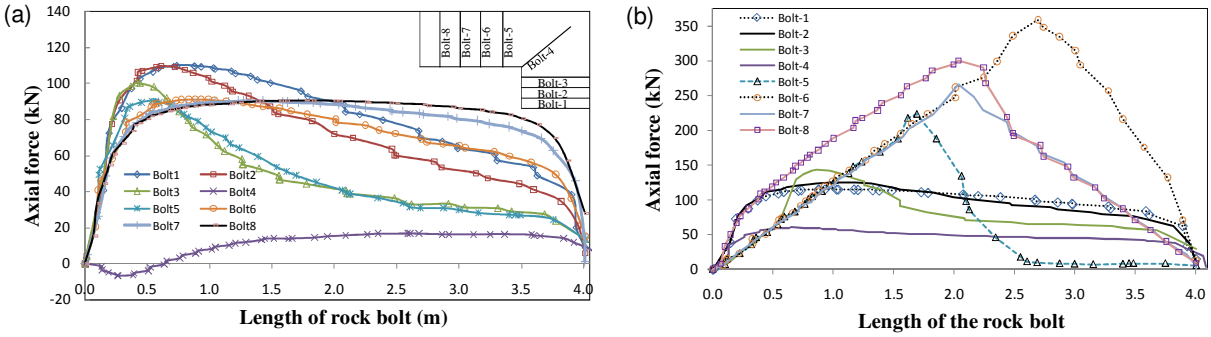

Fig.10 - Distribution of axial force on (a) coupled rock bolt and elastic rock mass (b) decoupled rock bolt and elasto-plastic rock mass around a rectangular opening

The maximum axial force of 110 kN is obtained by the coupled bolts in elastic rock mass for bolt numbers 1, 2 and 3 which are oriented horizontally. The distribution of shear stress and axial force along the decoupled bolt with elasto-plastic rock mass are illustrated in Figs. 10(b) and 11(b). The shear failure at the bolt-grout interface results in a release of the restrained rock deformation at near end of the tunnel boundary. After decoupling, location of neutral point moves inside the rock mass from the tunnel

wall. Due to asymmetrical stress distribution near the tunnel boundary, location of neutral point and maximum bolt force are also asymmetrical as listed in Table 3. The maximum axial force of 358 kN occurs at the bolt number 6 in elasto-plastic rock mass having decoupled rock-grout interface. At the same time, anchor length decreases from 3.12 m to 1.81 m for the same bolt.

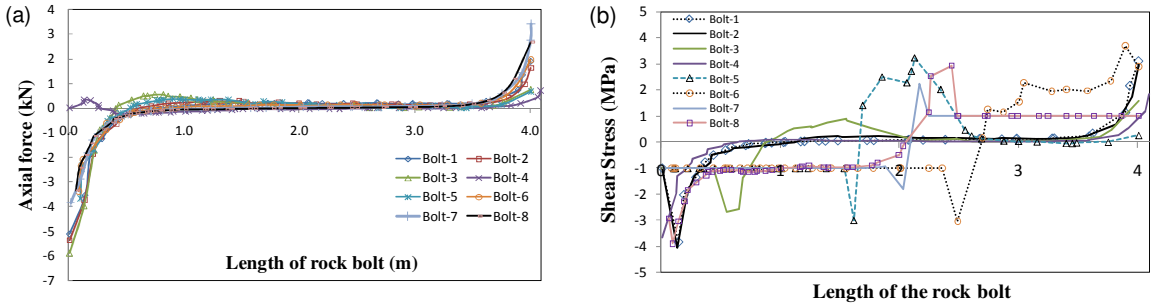

Fig. 11 - Distribution of shear stress on (a) coupled rock bolt and elastic rock mass (b) decoupled rock bolt and elasto-plastic rock mass around a rectangular opening

4.3 D-Shaped Tunnel

In this example, a D-shape tunnel with cross sectional area of 72 m^2 (almost equal as circular and rectangular tunnel) opening dimension of 11.36 m length and the maximum height of 7.1 m has been considered as shown in Fig. 5. The model geometry, finite element mesh and boundary conditions are shown in Fig. 12. Since the opening is axisymmetric with respect to vertical axis only, one half of the D-shaped tunnel has been modelled. The model is developed with 5859 CST elements having 3011 nodes and 8 bolts are installed around opening face at regular interval from the horizontal axis. Bolts positions are shown in Fig. 13(a) (inset-left top).

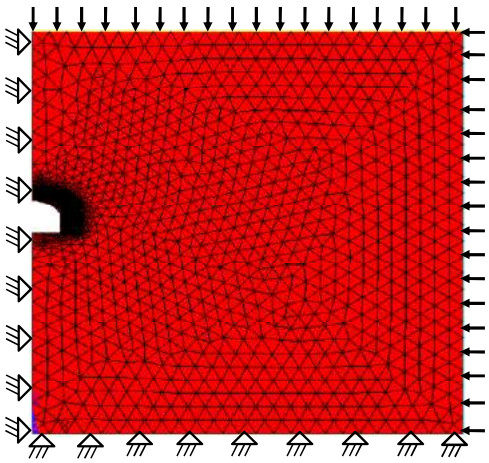

Fig. 12 - FE meshed for D-shape tunnel with uniform far field stress and boundary conditions

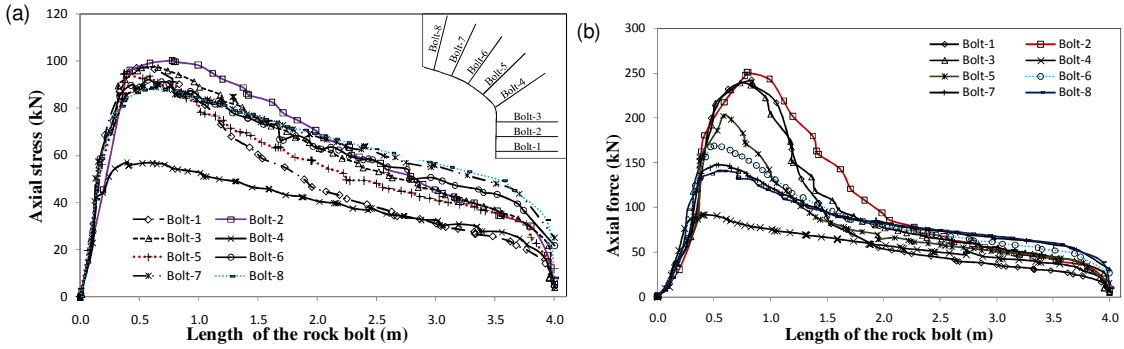

Fig. 13 - Distribution of axial force on (a) coupled rock bolt and elastic rock mass (b) decoupled rock bolt and elasto-plastic rock mass around a D-shaped opening

Figures 15(a) and 15(b) show the maximum axial force of different bolts for both coupled and decoupled conditions respectively. It is observed that maximum axial force for D-shape tunnel attains the higher value as compared to circular and rectangular openings. The maximum anchoring length of the bolts is also higher for D-shape. The maximum bolt anchoring length of 3.37 m is found in D-shaped opening as compared to 3.2 m for circular and 2.48 m for rectangular opening. It is found that the inclined bolt (Bolt-4) in rectangular and D-shaped opening does not perform as good as horizontal and vertical bolts. This may happen because variation in displacement of rock mass along the inclined distance is minimal.

Table 3 - Maximum axial force and position of neutral point of rock bolt in different opening and bolt position (number)

Bolt number			1	2	3	4	5	6	7	8
Circular	Elastic rock mass and coupled bolt	Maximum axial force (kN)	101	101	101	101	101	101	101	101
		Neutral point (m)	0.49	0.49	0.49	0.49	0.49	0.49	0.49	0.49
	Elasto-plastic rock mass and decoupled bolt	Maximum axial force (kN)	182	182	182	182	182	182	182	182
		Neutral point (m)	1.20	1.20	1.20	1.20	1.20	1.20	1.20	1.20
Rectangular	Elastic rock mass and coupled bolt	Maximum axial force (kN)	110	109	110	17	90	92	90	90
		Neutral point (m)	0.73	0.61	0.42	2.50	0.54	0.88	1.27	1.75
	Elasto-plastic rock mass and decoupled bolt	Maximum axial force (kN)	115	125	143	60	223	358	266	300
		Neutral point (m)	1.03	1.12	0.86	0.65	1.69	2.69	2.03	2.03
D-Shape	Elastic rock mass and coupled bolt	Maximum axial force (kN)	97	100	97	57	95	92	90	88
		Neutral point (m)	0.48	0.77	0.65	0.40	0.37	0.56	0.65	0.58
	Elasto-plastic rock mass and decoupled bolt	Maximum axial force (kN)	242	250	240	92	202	168	147	140
		Neutral point (m)	0.83	0.79	0.74	0.41	0.58	0.50	0.54	0.58

4.3.1 Results and discussions

Distribution of axial force and shear stress along the bolt length are plotted in Figs. 13(a) and 14(a) for elastic rock mass and coupled bolt. Figures 13(b) and 14(b) show axial force and shear stress for elasto-plastic rock mass and decoupled bolts. Again, asymmetrical bolt stress (axial and shear) are observed due to asymmetrical distribution of stresses in the rock mass. Neutral point location and the maximum axial force for each bolt are given in Table 3. Figure 13 shows that horizontal bolts (bolt-1, 2 and 3) take more loads as compared to others in both the cases (coupled with elastic rock mass and decoupled with elasto-plastic rock mass).

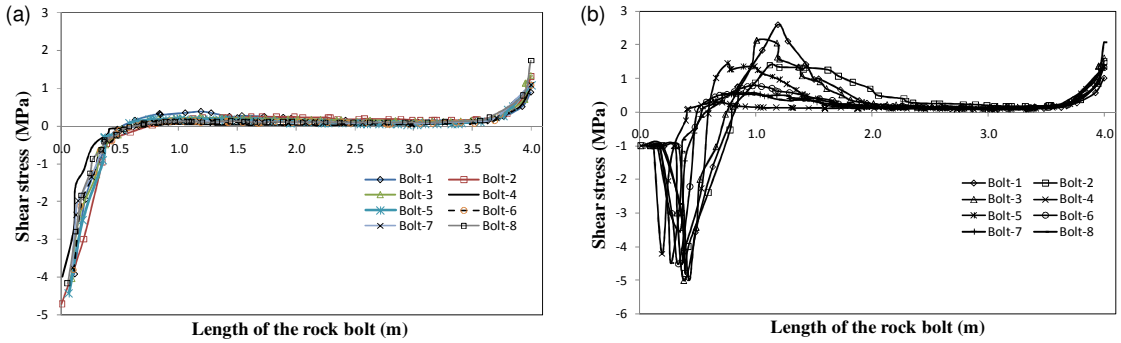

Fig. 14 - Distribution of shear stress on (a) coupled rock bolt and elastic rock mass (b) decoupled rock bolt and elasto-plastic rock mass around a D-shaped opening

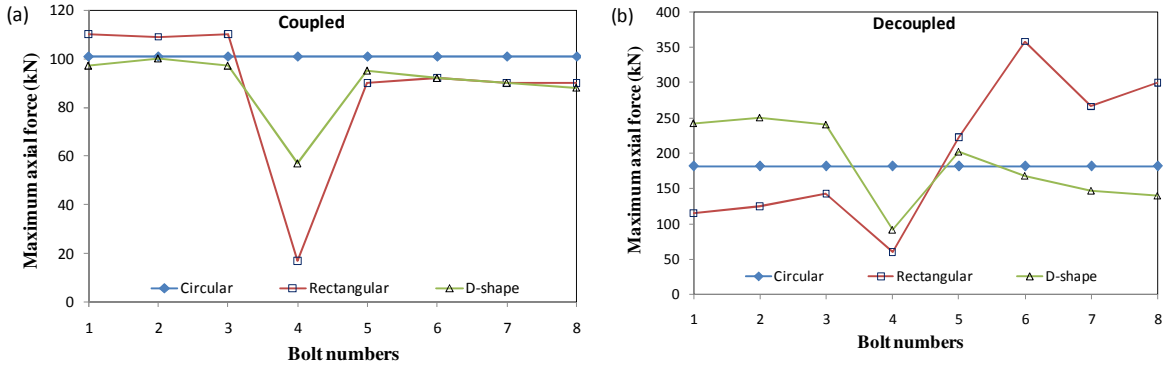

Fig. 15 - Maximum axial force for different bolt number (a) coupled rock bolt and elastic rock mass (b) decoupled rock bolt and elasto-plastic rock mass

The distribution of shear stress along the coupled bolt with elastic rock mass and decoupled bolt with elasto-plastic rock mass are illustrated in Figure 14(a) and 14(b) respectively. It has been observed that, the maximum and minimum decoupled length of 0.33 m occurs for bolt-1 and of 0.11 m occur for bolt-4 respectively.

5. CONCLUSIONS

This paper proposes applications of enriched finite element (EFEM) procedures for analyzing interaction between grouted rock bolt and rock mass. Three different shapes

of bolted tunnel have been analyzed in elastic rock mass with coupled and elasto-plastic rock mass with decoupled bolts. The salient features and specific conclusions of this study are summarized below:

- Bolt can be inserted at any location in a finite element mesh. It needs not have to be oriented along the nodes. Elements intersected by a bolt are enriched and the rest are regular.
- Bolt behaviour (load capacity, shear stress distribution etc) depends on shape of the opening and location of the bolt.
- The maximum axial force more if decoupling with rock failure is considered. The average maximum axial force has occurred for coupled bolt with elastic rock mass 1) 101 kN for circular 2) 88.5 kN for rectangular tunnel 3) 89.5 for D-shape tunnel. The average maximum axial force has occurred for decoupled bolt with elasto-plastic rock mass 1) 182 kN for circular 2) 199 kN for rectangular tunnel 3) 185 kN for D-shape tunnel.
- Location of neutral point after decoupling are 1.20 m for circular shape, 1.51 m (average) for rectangular shape and 0.62 m (average) for D-shape tunnel respectively.
- These results suggest that performance of bolt in terms of reinforcement is the best in D-shape tunnel as compared to other two tunnels. It has been observed that average anchoring length is also higher in D-shape tunnel indicating better bolt performance.

It may also be concluded that for better understanding of bolt behaviour more numerical models need to be analyzed considering different shapes of tunnel along with field monitoring of bolts.

References

Brady, B. and Lorig, L. (1988). Analysis of rock reinforcement using finite difference methods, Computers and Geotechnics, 5, 2, pp 123-149.

Cai, Y., Esaki, T. and Jiang, Y. (2004). A rock bolt and rock mass interaction model, International Journal of Rock Mechanics and Mining Sciences, 41, pp 1055-1067.

Carranza-Torres, C. (2004). Elasto-Plastic Solution Tunnel Problems Using Generalized Form of The Hoek-Brown Failure Criterion, SINOROCK 2004 2B 28, Beijing; International Journal of Rock Mechanics and Mining Sciences, 41, pp 629-639.

Carranza-Torres, C. and Fairhurst, C. (1999). The Elasto-plastic response of underground excavations in rock masses that satisfy the Hoek-Brown failure criterion, International Journal of Rock Mechanics and Mining Sciences, 36, pp 777-809.

Crotty, J.M. and Wardle, L.J. (1985). Boundary integral analysis of piecewise homogeneous media with structural discontinuities, International Journal of Rock Mechanics and Mining Sciences and Geomechanics Abstract, 22, 6, pp 419-427.

Cundall, P.A. (1971). A computer model for simulating progressive, large scale movements in blocky rock systems, ISRM Sym, 1, 8, pp 129-136.

d'Avila, V.M.R., Bristto, D.S. and Bittencourt, E. (2008). Numerical simulation of cracking in reinforced concrete members by an embedded model Engineering Computations, International Journal for Computer-Aided Engineering and Software, 25, 8, pp 739-763.

Deb, D. (2006). Finite Element Method Concepts and Applications in Geomechanics, Preentice Hall, New Delhi.

Deb, D. and Das, K.C. (2009). Extended Finite Element Method (XFEM) for Analysis of Cohesive Rock Joint, Journal of Scientific and Industrial Research, 68, 7, pp 575-583.

Deb, D. and Das, K. C. (2010). Enriched Finite Element Procedures for Interaction between Fully Grouted Decoupled Rock Bolts and Rock Mass, International Journal for Numerical and Analytical Methods in Geomechanics, Vol. 35, No. 15, pp.1636-1655.

Deb, D. and Das, K.C. (2010b). Extended Finite Element Method for the Analysis of Discontinuities in Rock Masses, Geotechnical and Geological Engineering, Springer, 28, 5, pp. 643-659.

Deb, D. and Choi, S.O. (2005). Singularity adjustment on generalized Hoek and Brown yield surface for elastic-plastic analysis, Proc. 40th U.S. Rock Mechanics Symposium, June, Anchorage, Alaska.

Elwi, A.E. and Hrudey, M. (1989). Finite element model for curved embedded reinforcement, Journal of Engineering Mechanics (ASCE), 115, 4, pp 740-754.

Goodman, R.D., Taylor, R.L. and Brekke, T. L. (1968). A model for the mechanics of jointed rock, Journal of the Soil Mechanics and Foundation division, ASCE, 14, pp 637-659.

Hyett, A.J., Moosavi, M. and Bawden, W.F. (1996). Load Distribution along Fully Grouted Bolts with Emphasis on Cable Bolt Reinforcement, International Journal of Numerical and Analytical methods in Geomechanics, 20, pp 517-544.

Indraratna, B. and Kaiser, P.K. (1991). Analytical model for the design of grouted rock bolt, International Journal of Numerical and Analytical methods in Geomechanics, 14, pp 227-251.

Itasca (2005). FLAC - Fast Lagrangian Analysis of Continua, Itasca Consulting Group Inc., Minneapolis, USA, Version 5.0.

Li, C. and Stillborg, B. (1999). Analytical model for rock bolts, International Journal of Rock Mechanics and Mining Sciences, 36, pp 1013-1029.

Marence, M. and Swoboda, G. (1995). Numerical Model for Rock Bolts with Consideration of Rock Joint Movements, Rock Mechanics and Rock Engineering, 28, 3, pp 145 165.

Pande, G.N., Beer, G. and Williams, J.R. (1990). Numerical Methods in Rock Mechanics, John Wiley and Sons Publisher, New York.

Rockscience (2005). Finite Element Analysis and Support Design - Phase 2, Geomechanics software and Research, Rockscience Inc., Toronto, Ontario, Canada.

Sharan, S.K. (2003). Elastic-Brittle-Plastic Analysis of Circular Openings in Hoek-Brown Media, International Journal of Rock Mechanics and Mining Sciences, 40, pp 817-824.

Snyder, W.V. (1983). Analysis of beam building using fully grouted roof bolts, Int. Symp. on Rock Bolting, Sweden, pp 246-255.

Stille, H. (1992). Rock support in theory and practice, Int. Symp. of Rock Support in Mining and Underground Construction, Canada, pp 421-437.

Stille, H., Holmberg, M. and Nord, G. (1989). Support of weak rock with grouted bolt and shotcrete, International Journal of Rock Mechanics and Mining Sciences and Geomechanics, 26, pp 99-113.

Windsor, C.R. and Thompson, A. (1993). Rock reinforcement technology, testing design and evaluation, Compressive Rock Engineering Principals, Practice and Projects (Ed. J.A. Hudson), Vol. 4, pp 451-484.

Windsor, C. R. and Thompson, A. (1996). Terminology in rock reinforcement practice, NARAMA96, Canada.